Lysimeter based evaporation and condensation dynamics in a Mediterranean ecosystem

Sinikka J. Paulus[1], Tarek S. El-Madany[1], René Orth[1], Anke Hildebrandt[2,3], Thomas Wutzler[1], Arnaud Carrara[4], Gerardo Moreno[5], Oscar Perez-Priego[6], Olaf Kolle[1], Markus Reichstein[1], and Mirco Migliavacca[1,7]

[1]Max Planck Institute of Biogeochemistry, Jena, Germany
[2]Helmholtz Centre for Environmental Research - UFZ, Department Computational Hydrosystems, Leipzig, Germany
[3]Friedrich-Schiller University, Group Terrestrial Ecohydrology, Jena, Germany
[4]Fundacion Centro de Estudios Ambientales del Mediterraneo, Valencia, Spain
[5]Universidad de Extremadura, INDEHESA - Institute for Silvopastoralism Research, Plasencia , Spain
[6]Universidad de Córdoba, Department of Forestry Engineering, Córdoba, Spain
[7]now at: European Commission Joint Research Centre, via E. Fermi 2479, Ispra, Italy

Correspondence: Sinikka Paulus (spaulus@bgc-jena.mpg.de)

Abstract.

The input of liquid water to terrestrial ecosystems is composed of rain and non-rainfall water input (NRWI). The latter comprises dew, fog, and adsorption of atmospheric vapor on soil particle surfaces. Although NRWIs can be relevant to support ecosystem functioning in seasonally dry ecosystems, they are understudied, being relatively small, and therefore hard to mea-

5   sure. In this study, we test a routine for analyzing lysimeter data specifically to determine NRWI. We apply it on one year of data from large high-precision weighing lysimeters at a semi-arid Mediterranean site and quantify that NRWIs occur for at least $3\,\mathrm{h}$ on 297 days (81 % of the year) with a mean diel duration of $6\,\mathrm{hours}$. They reflect a pronounced seasonality as modulated by environmental conditions (i.e., temperature and net radiation). During the wet season, both dew and fog dominate NRWI, while during the dry season it is soil adsorption of atmospheric vapor. Although NRWI contributes only 7.4 % to the annual

10   water input NRWI is the only water input to the ecosystem during $15\,\mathrm{weeks}$, mainly in the dry season. Benefitting from the comprehensive set of measurements at the Majadas instrumental site, we show that our findings are in line with (i) independent model simulations forced with (near-) surface energy and moisture measurements and (ii) eddy covariance-derived latent heat flux estimates. This study shows that NRWI can be reliably quantified through high-resolution weighing lysimeters and a few additional measurements. Their main occurrence during night-time underlines the necessity to consider ecosystem water fluxes

15   at high temporal resolution and with 24-hour coverage.

1 Introduction

Water availability at the land surface controls a variety of processes related to land-atmosphere exchange, such as the warming of the surface and air temperature (T_a, $°C$) (Seneviratne et al., 2010; Panwar et al., 2019), ecosystem carbon fluxes (Reichstein et al., 2007; El-Madany et al., 2021), and evapotranspiration (ET, mm) (Jung et al., 2010; Rodriguez-Iturbe et al.,

20   2001). Therefore, precise quantification of the water balance is crucial for understanding and simulating these processes. The largest atmospheric input of liquid water to ecosystems globally is rain. In addition, other liquid water inputs exist, which are summarized under the term non-rainfall water input (NRWI).

NRWIs comprise several types of processes: deposition (fog, horizontal precipitation), condensation (formation of dew, soil distillation, and hoar frost), and soil vapor adsorption (Kidron and Starinsky, 2019). These processes are mainly controlled
25   by i) atmospheric vapor pressure (e_a, hPa), ii) surface temperature (T_s, $°C$) and iii) topsoil water potential. Fog is defined as water droplets suspended in the air at a concentration that reduces visibility below $1000\,\mathrm{m}$ (Feigenwinter et al., 2020). The droplets adhere to surfaces after contact. This fog deposition is commonly derived from relative humidity (rH, %) or visibility measurements (Feigenwinter et al., 2020; Zhang et al., 2019b). Condensation processes are induced by T_s decreasing below the dewpoint temperature (T_{dew}, $°C$) of nearby air. This is referred to either as dew when the water originates from
30   the atmosphere, or soil distillation when the water originates from the soil beneath. However, differentiating between these two origins is commonly not possible (Li et al., 2021b) and most literature summarizes both processes as dew. Dew is often measured with lysimeters (Meissner et al.; Groh et al., 2018; Zhang et al., 2019b) or by leaf wetness sensors (Feigenwinter et al., 2020).

In contact with soil, the water vapor is influenced by capillary and adsorptive forces due to pore shapes and the polarity of the solid material (Tuller et al., 1999). These forces increase in relevance as the soil dries out. They reduce the saturation
35   vapor pressure as a function of soil dryness (Edlefsen et al., 1943), leading to condensation within the soil at rH lower than $100\,\%$. The respective NRWI is the adsorption of atmospheric vapor. However, despite being well understood at pore and laboratory scales (Tuller et al., 1999; Arthur et al., 2016), this process was underrepresented in NRWI studies (Zhang et al., 2019b; Saaltink et al., 2020; Kohfahl et al., 2019).

So far, no standard technique has been developed to measure the different components of NRWI in the field. Partly, this
40   is related to technical limitations in measuring capabilities (summarized in Feigenwinter et al., 2020). Modeling NRWI also remains a challenge, although a distinction must be made between modeling frequency and duration, and modeling the yields of the different NRWI fluxes. In the case of dew for example fewer studies have addressed the development of the latter models due to the overall complexity of heat and radiation exchange and many unknown necessary parameters (Tomaszkiewicz et al., 2015). The same is true for adsorption (Verhoef et al., 2006).

45   Furthermore, the relatively small contribution of NRWI for the annual water balance lead to an underestimation of their relevance for ecosystem functioning. But NRWI subsidies can extend or sustain ecosystem functioning when rain and soil moisture are low (Weathers et al., 2020; Tomaszkiewicz et al., 2015). This is long known for arid ecosystems (Duvdevani, 1963; Agam and Berliner, 2006; Kidron and Starinsky, 2019) but an increasing number of studies suggest ecological relevance
50   also in the context of seasonal dry spells (Jacobs et al., 2006; Li et al., 2021b; Groh et al., 2018; Dawson and Goldsmith, 2018). As leaf wetting events, dew and fog can affect leaf water status directly and alter the surface water and energy balance by changing leaf temperature, albedo, and water vapor deficit (Dawson and Goldsmith, 2018; Gerlein-Safdi et al., 2018; Aparecido et al., 2017). Uptake of water at the leaf surface was observed across ecosystems, species, and plant types relieving daily water and carbon stress (Dawson and Goldsmith, 2018; Berry et al., 2014; Aparecido et al., 2017). Secondary effects of

55   NRWIs related to changes in canopy micro-climate have also been shown to reduce plant water stress and increase water use
efficiency (Ben-Asher et al., 2010). Respiration in dry seasons of organisms like biocrusts (Kidron and Kronenfeld, 2020a),
microbes within the soil (McHugh et al., 2015), and on standing litter (Evans et al., 2019; Gliksman et al., 2017) was sustained
due to dew and adsorption. Nevertheless, the role of NRWIs in connection with the carbon cycle across ecosystems has not yet
been fully understood and quantified (Dawson and Goldsmith, 2018; Weathers et al., 2020; Kidron and Starinsky, 2019).

60   Research about the role of NRWI remains limited by too few measurements of their actual amounts (Berry et al., 2019).
Appropriate measurement facilities to analyze and quantify the local circumstances of NRWI occurrence seem sparse. Past
studies were often based on micro-lysimeters covering time periods of few weeks to some months. Recently Kidron and
Kronenfeld (2020b) found that temperature inside the micro-lysimeters deviated from that in the surrounding soil, and also that
instrument structure, such as column length and parent material, were impacting flux sums. These issues are partly overcome

65   for large high precision weighing lysimeters, where lower boundary control systems were developed which equilibrate soil
temperature and moisture content between the inside of the lysimeter and the surrounding soil to prevent biases (Groh et al.,
2016). Therefore, data collected with large weighing lysimeters can further contribute to the identification and quantification
of NRWIs. Yet, relatively few stations are located in semi-arid and arid environments (Perez-Priego et al., 2017; Dijkema et al.,
2018; Kohfahl et al., 2019; Zhang et al., 2019b) where NRWIs are expected to be particularly relevant.

70   In this study, we implement and test a processing scheme for identifying and quantifying NRWIs in a seasonally dry ecosys-
tem in continental Spain. The aims of this paper are to (i) extend and refine processing routines for water flux partitioning
to distinguish between ET, rain, and individual NRWIs, based on lysimeter and meteorological data; (ii) analyze the seasonal
NRWI dynamics and their contribution to the annual water input at the site; and (iii) evaluate our results against independent
observations and empirical models.

75   2   Material and Methods

2.1   Study site

All data investigated in this study originates from the experimental field site Majadas de Tietar, Caceres in Extremadura, Spain
(39°56′25.12″ N, 5°46′28.70″ W). Average diel T_a is 16.7 °C with diel minimum and maximum T_a of 3.1 °C to 12.5 °C
in January and 18.6 °C to 39.8 °C in August. The rain mainly falls between October and April, with mean annual amounts

80   of ca. 650 mm, with large interannual variations (El-Madany et al., 2020). The ecosystem is a typical Mediterranean semi-
arid tree-grass ecosystem (*Dehesa*) with low-density oak tree cover (*Quercus Ilex* (L.),   20 trees ha^{-1}) (Bogdanovich et al.,
2021). The herbaceous layer consists of native annual grasses, forbs, and legumes (Migliavacca et al., 2017) with a seasonally
varying fractional cover mainly influenced by moisture availability (Luo et al., 2020). The growing season for the herbaceous
layer begins after the first rains after summer (typically in mid-October) and is inhibited by low temperatures in winter before

85   peaking in spring before the dry season. During the dry season, the herbaceous species are inactive until the return of rain
(Perez-Priego et al., 2018). The site is managed with low-intensity grazing by cows during the growing season (El-Madany
et al., 2018). An exclusion cage was used to avoid cows stepping into the lysimeters. However, the structure of the cage allowed

for grazing to maintain the lysimeters comparable with the rest of the plot. The soil is formed of alluvial deposits and classified as Abruptic Luvisol (IUSS Working Group WRB, 2015) with sandy topsoil of $74\,\%$ sand, $20\,\%$ silt, and $6\,\%$ clay (Nair et al.,
90 2019). A clay layer rests at a variable depth between $30\,\mathrm{cm}$ to $100\,\mathrm{cm}$. Although the trees also play a role in the water balance at the ecosystem scale, herbaceous vegetation dominates ET (Perez-Priego et al., 2017). This work focuses on the water fluxes in open areas where lysimeters are located (Migliavacca et al., 2017).

2.1.1 Lysimeter technical specifications

The site is equipped with three lysimeter stations, each containing two weighable high-precision lysimeters (UGT, Müncheberg,
95 Germany), for a total of 6 columns. Each column has a $1\,\mathrm{m}^2$ surface area and $1.20\,\mathrm{m}$ column depth. They rest of the weighing systems consisting of three precision shear-stress cells, respectively (Model 3510, Stainless Steel Shear Beam Load Cell, VPG Transducers, Heilbronn, Germany). The weight measurements are collected every $1\,\mathrm{min}$ with a measurement precision of $10\,\mathrm{g}$ ($0.01\,\mathrm{mm}$). Each lysimeter station is equipped with a lower boundary control system to avoid deviations from natural conditions due to the isolation of the lysimeter columns (Groh et al., 2016). Porous ceramic bars at the bottom of the lysimeters maintain
100 the soil water potential within the column comparable with the soil surrounding them. Soil temperature (T_{soil}, °C) is controlled with a heat exchange system (*for further details, see* Perez-Priego et al. (2017)). SWC and T_{soil} are measured every $15\,\mathrm{min}$ within the columns at 0.1, 0.3, 0.75, and $1\,\mathrm{m}$ depth (UMP-1, Umwelt-Geräte-Technik GmbH, Müncheberg, Germany). Soil matric potential (Ψ, hPa) is measured every $15\,\mathrm{min}$ at $0.1\,\mathrm{m}$ depth with a porous ceramic cone full range pF meter (ecoTech Umwelt-Meßsysteme GmbH, Bonn, Germany).
105 The stations were installed in 2015 at open grassland patches with 104 m, 91 m, and $24\,\mathrm{m}$ distance to each other, respectively. The closest tree is $\sim 9\,\mathrm{m}$ away. To test the application of data processing and flux classification across seasons, we analyze a period of one year from June 1st, 2019 to May 31st, 2020.

2.1.2 Ancillary measurements outside the lysimeters

For partitioning the lysimeter weight changes (ΔW, $\mathrm{kg\,min}^{-1}$) into different water fluxes and modeling (see Section 2.2.1,
110 2.3.1, and 2.3.2) we used additional field measurements collected every $30\,\mathrm{min}$. Meteorological variables monitored are rain, which is measured with a weighing rain gauge (TRwS 514 precipitation sensor, MPS systém, Slovakia), T_a, and rH at 1 m (Pt–100 capacitive humidity sensor CPK1–5, MELA Sensortechnik, Germany). T_{dew} was calculated based on T_a and rH (see Appendix A2). Actual vapor pressure (e_a, hPa) is calculated from T_a and rH.

Short- (SW, $\mathrm{W\,m}^{-2}$) and longwave (LW, $\mathrm{W\,m}^{-2}$) incoming ($\downarrow$) and outgoing ($\uparrow$) radiation of the herbaceous layer was
115 observed with a net radiometer (CNR4, Kipp and Zonen, Delft, Netherlands) at a measurement height of $\sim 2\,\mathrm{m}$. T_s is calculated from LW (equations in Appendix A2). Ground heat flux (G, $\mathrm{W\,m}^{-2}$) was monitored with soil heat flux plates (Heatflux Ramco HP3, McVan Instruments, Mulgrave, Australia).

T_{soil}, and SWC were measured along a profile outside the lysimeters at 0.05 m, 0.10 m, and $0.2\,\mathrm{m}$ depth, respectively (Delta-ML3, Delta-T Devices Ltd, Burwell Cambridge, UK).

120   Fluxes of latent heat (λE, $\mathrm{W\,m^{-2}}$), wind speed (u, $\mathrm{m\,s^{-1}}$) and friction velocity (u^*, $\mathrm{m\,s^{-1}}$) were measured by an eddy covariance (EC) system, consisting of a sonic anemometer (R3–50 Gill Instruments, Lymingon UK) and an infra-red gas analyzer (LI-7200, Licor Biosciences, Lincoln, USA) at $1.6\,\mathrm{m}$ sampling height and targeting the herbaceous layer (Perez-Priego et al., 2017). For further details on the EC data processing, see El-Madany et al. (2018).

2.2   Data analysis

125   ### 2.2.1   Lysimeter data processing

The processing of lysimeter data comprises several steps: (a) raw weight data filtering, (b) time-series smoothing, and (c) flux partitioning. The processing workflow is displayed in figure 1. All code used in the analysis is available for reproducibility in the open-source R environment for statistical programming (R Core Team, 2020). See the data and code availability statement for more details.

130   **a) Raw data processing:** changes in the water reservoir through the lower boundary system and lysimeter column weights are added together. Outliers are filtered out by setting plausible threshold values; $-0.5\,\mathrm{kg\,min^{-1}} < \Delta W < 1\,\mathrm{kg\,min^{-1}}$ (Schrader et al., 2013). Additionally, outliers within these threshold values were identified by comparing ΔW across the six columns. If ΔW is due to rain, we expect similar responses across lysimeters. In contrast, if only one lysimeter column shows an anomalous ΔW we considered this as an artifact (e.g., animal stepping on the column or issues with the boundary

135   control) that can be removed from the time series (Hannes et al., 2015). For identifying these values, we calculated the mean ΔW of all six lysimeters for an interval i of one minute. This value was then subtracted from the individual ΔW measurements during i. The resulting value is a normalized weight change ($\Delta \mathrm{W}_{\mathrm{normalized},i}$, kg) for each column. Then, an average standard deviation ($\overline{\sigma}$, kg) was calculated from $\Delta \mathrm{W}_{\mathrm{normalized},i-3}$ to $\Delta \mathrm{W}_{\mathrm{normalized},i+3}$. $\Delta \mathrm{W}_{\mathrm{normalized},i} > (1.5 \times |\overline{\sigma}|)$ are replaced by not a number (NA).

140   **b) Time-series smoothing:** is necessary to remove noise from the time series before the partitioning and data analysis based on ΔW (Schrader et al., 2013). Since noise in this type of data is not constant in time due to wind for example (Nolz et al., 2013), we apply a routine with adaptive averaging window widths (ω) and adaptive ΔW thresholds (δ) (AWAT) from Peters et al. (2014, 2016, 2017). As an intermediate result, the AWAT algorithm produces a step function of lysimeter weight. At last, a smoothing of the $1\,\mathrm{min}$ resolution time series is performed using a spline interpolation. We chose this routine because

145   the authors included a processing step developed specifically for dew conditions (Peters et al., 2017). In our application, the parameter ω varied between $3\,\mathrm{min}$ to $31\,\mathrm{min}$ and δ between $0.01\,\mathrm{mm}$ to $0.05\,\mathrm{mm}$. A detailed overview of the algorithm and an evaluation of the performance are compiled in Peters et al. (2017) and Hannes et al. (2015). If one out of all columns was measuring more than $16\,\mathrm{h}$ of water input during one day, the full day was excluded for the analysis for the respective column. Due to technical problems that became obvious after data processing, lysimeter column number 4 was completely excluded

150   from further analysis. After the smoothing, the time series are aggregated to a 5-minute resolution to further decrease the remaining influence of noise for the subsequent step of flux partitioning, particularly for values close to zero.
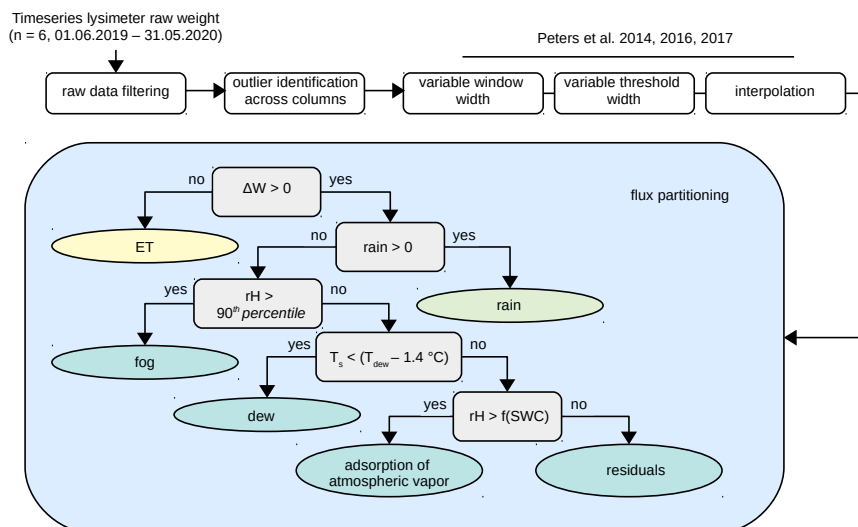
Figure 1. Overview of the lysimeter data processing to determine non-rainfall water inputs. White rectangles represent the steps of the pre-processing chain before flux partitioning. The pre-processed time series is then classified into the different vertical water fluxes based on a decision tree structure shown in the light blue box; grey rectangles stand for the decision nodes, and ellipses for the endpoint nodes. The decision tree is adapted from Zhang et al. (2019a).

c) **Flux partitioning:** the filtered time series of ΔW is divided into six different water fluxes, assuming that in 5-minute intervals, only one process prevails over the others. Negative ΔW is always classified as ET. Positive ΔW is separated into different flux categories in a decision tree structure considering additional meteorological data, as illustrated in figure 1. We use the convention that outgoing fluxes like ET take negative values (related to negative ΔW as water is leaving the soil), and rain and NRWIs are positive (because associated with positive ΔW). At the second decision node, we check if the rain gauge identifies a rain event during the period of weight increase. If true, all positive ΔW are classified as rain during $30\,\mathrm{min}$ before and after the event. This period was selected to match the measurement interval of rain gauges which is $30\,\mathrm{minutes}$. If false, e.g., in the absence of rain, rH is evaluated. If rH exceeded a threshold identified as the 90th percentile of the rH sensor records, ΔW is attributed to fog. In our case, this threshold value is at $rH_t = 97.8\,\%$ and measured by a sensor at $1\,\mathrm{m}$ height. We decided to set a rH threshold that is based on the data distribution of the sensor because it accounts for the individual uncertainty which is particularly high when the air is nearly saturated (Feigenwinter et al., 2020), systematic biases, and drifts of rH sensors.

If neither fog nor rain is detected, we compared T_s with T_{dew} at $1\,\mathrm{m}$ sensor height (equations in Appendix A2). Note that this is not necessarily representative of T_{dew} within the grass canopy, which would be more suitable to infer dew formation. For example, through radiative cooling, the air cools faster closer to the surface than at $1\,\mathrm{m}$ height. To include the effect of the height difference, we compared sensors installed at $0.1\,\mathrm{m}$ and at $1\,\mathrm{m}$ height during a measurement campaign of two months in

Spring 2021. The results show that the median temperature difference between the $0.1\,\mathrm{m}$ to $1\,\mathrm{m}$ sensor height is $1.4\,°\mathrm{C}$ with an IQR of $1.2\,°\mathrm{C}$. Dew was therefore assigned when $T_s < (T_{dew} - T_{dew,t})$ where $T_{dew,t}$ is set to $1.4\,°\mathrm{C}$.

170 If no dew was detected, ΔW could be potentially attributed to soil adsorption of atmospheric vapor (Zhang et al., 2019a). Adsorption occurs, however, at specific soil hydraulic and meteorological conditions given by a relation between Ψ and atmospheric rH. Those have been observed in the laboratory (Camuffo, 1984; Arthur et al., 2016) and suggested from field observations (Kosmas et al., 2001; Uclés et al., 2015; Zhang et al., 2019b). For adsorption Ψ falls below (or is less negative than) a given threshold. This threshold can also be expressed in terms of SWC, given the relationship between Ψ and SWC

175 through the soil water retention curve. In order to integrate this knowledge into the classification of adsorption, measurements of rH and SWC were analyzed for the periods where adsorption conditions were identified based on modeling (see section 2.3.2). For these periods, we fit a nonlinear quantile regression (90th *percentile*) to measurements of rH and SWC. This nonlinear relationship is depicted in Appendix Fig. A1. Although for the description of this relationship multiple empirical functions exist for samples measured in the laboratory under equilibrated conditions, they do not apply to our case due to the

180 different observation ranges of rH and SWC at our site (see Fig. A1 for examples). When $rH \geq f(SWC)$, soil adsorption of atmospheric vapor is assigned to positive ΔW. When $rH < f(SWC)$ we classify the flux as residual.

The results of the partitioning algorithm, as well as the uncertainty of the NRWIs might be sensitive to the set of parameters and thresholds values used at each node. Therefore, the impact of the choice of threshold parameters on the flux uncertainty was tested. To do so, we defined a parameter set that describe the upper and lower limit of the parameter values, specifically

185 rH_t = [80, 100] % and $T_{dew,t}$ = [0, 1.5] °C. The parameter values tested cover the ranges of threshold values for rH and T_s which are currently used in similar studies to identify fog and dew conditions (e.g., Feigenwinter et al., 2020; Zhang et al., 2019b). We then ran forward the partitioning algorithm with all the combinations of the parameters. The uncertainty of the calculated fluxes was then characterized based on the interquartile range (IQR) of the resulting flux quantities as will be shown in Section 3.1.

190 **2.3   Comparing rain and evapotranspiration against independent observations and derived NRWI against models predictions**

We test the plausibility of inferred water fluxes by three different methods: 1) qualitative and quantitative comparison against direct measurements of rain and ET and 2) comparison against model predictions of dew and adsorption in absence of respective direct measurements derived with alternative measured variables. Similar approaches were used successfully for the

195 benchmarking of methods to simulate transpiration (Nelson et al., 2018) or carbon fluxes (Jung et al., 2020). Measured flux durations were compared to respective model estimates modeled flux using correlation, mean absolute error (MAE), and root mean squared error (RMSE) (full equations Appendix A2). 3) for periods classified as fog by the partitioning algorithm we cross check with images collected by a digital camera installed at the site (Luo et al., 2018). This was, however, only applicable for few events, since the first image per day was taken at 10 am.

2.3.1 Modelling dew

Dew is modeled as negative latent heat flux calculated based on models originally developed for determining evapotranspiration: (i) the Penman-Monteith (PM) (Monteith, 1965) equation which combines processes related to radiative energy and vapor pressure deficit (previously applied for dew in various forms by e.g. Jacobs et al., 2006; Aguirre-Gutiérrez et al., 2019; Groh et al., 2018), and (ii) equilibrium evaporation (previously applied for dew by Uclés et al., 2014).

We implemented the models as described in Ritter et al. (2019) and Jacobs et al. (2006) (Eq. (2.1)) and in Uclés et al. (2014) (Eq. (2.2)).

$$
\lambda E = \frac{s}{s+\gamma} \times (R_{net} - G) + \frac{\gamma}{s+\gamma} \frac{\rho_a \, \gamma \, \delta q}{r_{av}} \tag{2.1}
$$

$$
\lambda E = \frac{s \, (R_{net} - G)}{s+\gamma} \tag{2.2}
$$

where λE $(\mathrm{W\,m^{-2}})$ is the latent heat, s $(\mathrm{Pa\,K^{-1}})$ is the slope of the specific saturation curve, γ $(\mathrm{Pa\,K^{-1}})$ is the psychrometric constant, R_{net} is net radiation $(\mathrm{W\,m^{-2}})$, G is the soil heat flux $(\mathrm{W\,m^{-2}})$, ρ_a $(\mathrm{kg\,m^{-3}})$ is the density of air, and δq is the deficit of specific humidity at reference level $(\mathrm{kg\,kg^{-1}})$. r_{av} is the aerodynamic resistance to vapor transport between the surface and the air $(\mathrm{s\,m^{-1}})$ and was derived with an empirical relationship based on u^* (Thom, 1972).

For both equations, dew occurs when $\lambda E < 0$ and $T_s \leq (T_{dew} - 1.4\,^\circ\mathrm{C})$ (as explained in section 2.2.1). This approach has been reported to be suitable for detecting potential dew conditions and to analyze dew frequency and duration. But it is limited in reproducing dew yields (Ritter et al., 2019). Hence we focus on comparing condition lengths rather than yields since we aim to validate dew detection by the partitioning routine.

2.3.2 Modelling adsorption

Adsorption conditions were identified based on the vertical humidity gradient near the surface. We implemented the re-arranged aerodynamic diffusion equation originally used by Milly (1984) and previously applied for modeling adsorption by Verhoef et al. (2006):

$$
e_{s,0} = \frac{\gamma \, r_{av} \, \lambda E}{\rho_a \, C_p} + e_a \tag{2.3}
$$

The target value $e_{s,0}$ (kPa) is vapor pressure of soil air at the surface. e_a (kPa) is vapor pressure of the atmosphere and C_p $(\mathrm{J\,kg^{-1}\,K^{-1}})$ is the specific heat of air at constant pressure. The other parameters are the same as in Eq. (2.1). When $e_{s,0} < e_a$, gradient driven vapor flow is towards the soil surface. This is assumed to be indicative of the adsorption of vapor from the atmosphere. Different from the dew models, we used high-quality filtered measurements from EC for λE in Eq. (2.3). Again, we only compared the simulated daily duration of suitable conditions of atmospheric adsorption against the results obtained with the lysimeter weights partitioning and we constrained the comparison to moments when $T_s \leq (T_{dew} - 1.4\,^\circ\mathrm{C})$.

3 Results

3.1 Diurnal and seasonal changes of water fluxes
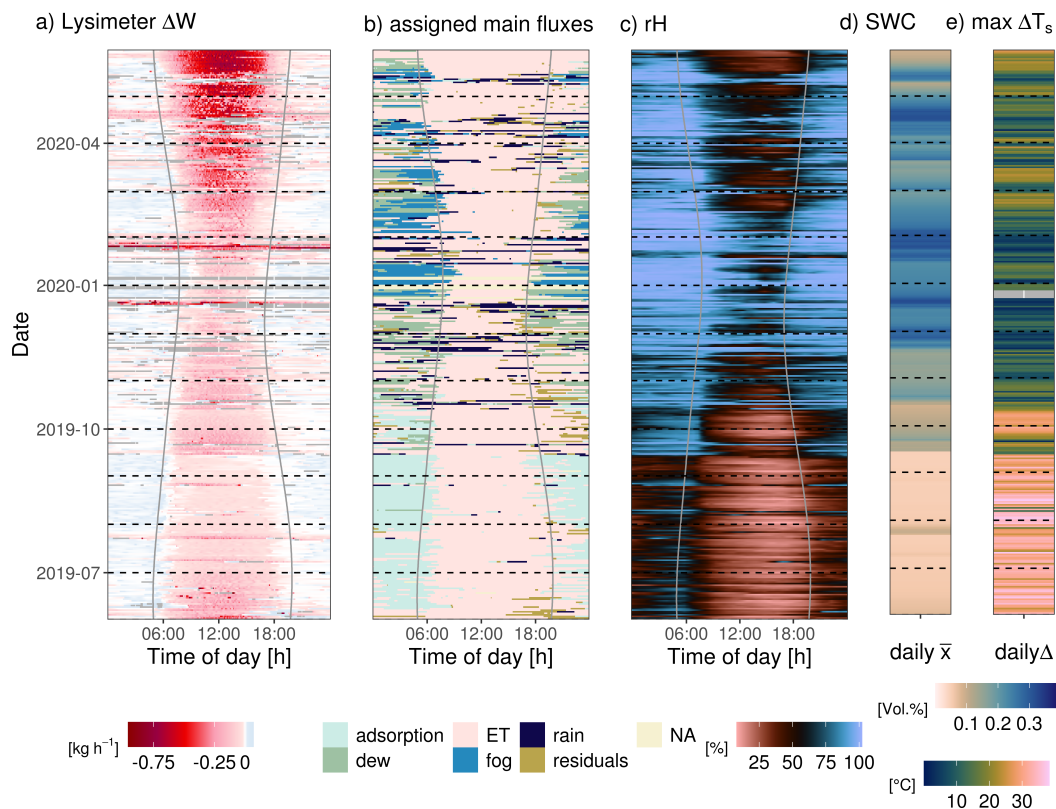
Figure 2. Diel and seasonal dynamics of a) lysimeter weight changes, b) assigned flux types, both from lysimeter 6, c) rH measured at $1\,\mathrm{m}$ height. Solid vertical lines mark sunrise and sunset, respectively, determined with the geographic coordinates of the field site. Mean SWC at $0.05\,\mathrm{m}$ depth and maximum diel difference of T_s are displayed as diel measurements in panels d) and e).

230   Figure 2 shows the fingerprint of lysimeter ΔW induced by ET, rain, and NRWI, assigned water flux types (exemplarily shown for lysimeter column 6) and rH, respectively, together with mean diel SWC at $0.05\,\mathrm{m}$ depth and maximum diel T_s range.

     Lysimeter ΔW are mainly negative between sunrise and sunset (Fig. 2a), e.g., water is lost from the column due to ET. After sunset, however, they are zero or positive during most of the year, indicating water input. This diel pattern is consistent

235 across seasons, following the seasonal daylight variability. The flux classification reveals seasonal differences in the prevailing NRWI (Fig. 2b). At the beginning of June, atmospheric adsorption mainly occurs during the early morning, before sunrise. From July to September the length of the adsorption period increases, and the onset shifts towards earlier in the night. In this

period, the diel variability of rH is relatively low (Fig. 2c), SWC at $5\,\mathrm{cm}$ depth is below $10\,\%$ and T_s oscillates up to an amplitude of $35\,°\mathrm{C\,day^{-1}}$ (Fig. 2d & e). A rain event, in late July increases SWC and is followed by some days of increased
240   ET which also prevails during night-time.

A rain event in late September leads to longer-lasting increases in SWC and rH. Such conditions are typically associated with vegetation re-greening. ET and dew alternate during night-time. Frequent rain events in November and December are accompanied by dew and fog becoming the dominant NRWIs until the end of the measurement period in April.

NRWI occur for at least $3\,\mathrm{h}$ during $297\,\mathrm{days}$ ($81\,\%$ of the year) with a mean duration of 6 hours per day of occurrence.

245   The weekly sums in Fig. 3 illustrate that the seasonal dynamics are consistent across lysimeters. The ecosystem receives atmospheric water at any time of the year but with shifting relative relevance of the water flux types over the year. Rain is the dominant liquid water input (i.e. it contributes more than $50\,\%$ of the weekly water input) during $29\,\mathrm{weeks}$ since it's total amount is usually much greater than NRWI, whereas NRWI is dominant in $24\,\mathrm{weeks}$. They are even the only water input during $15\,\mathrm{weeks}$ with adsorption as exclusive water input in $10\,\mathrm{weeks}$ of the year. Dew and fog occurrence is synchronized with rain
250   with regard to the seasonal occurrence, and therefore their relative contribution is small. The median contribution of adsorption until September 2019 is $0.9\,\mathrm{mm\,week^{-1}}$. With ET amounting to $-5.7\,\mathrm{mm\,week^{-1}}$, thus adsorption compensates for $19\,\%$ of the weekly water loss during summer.
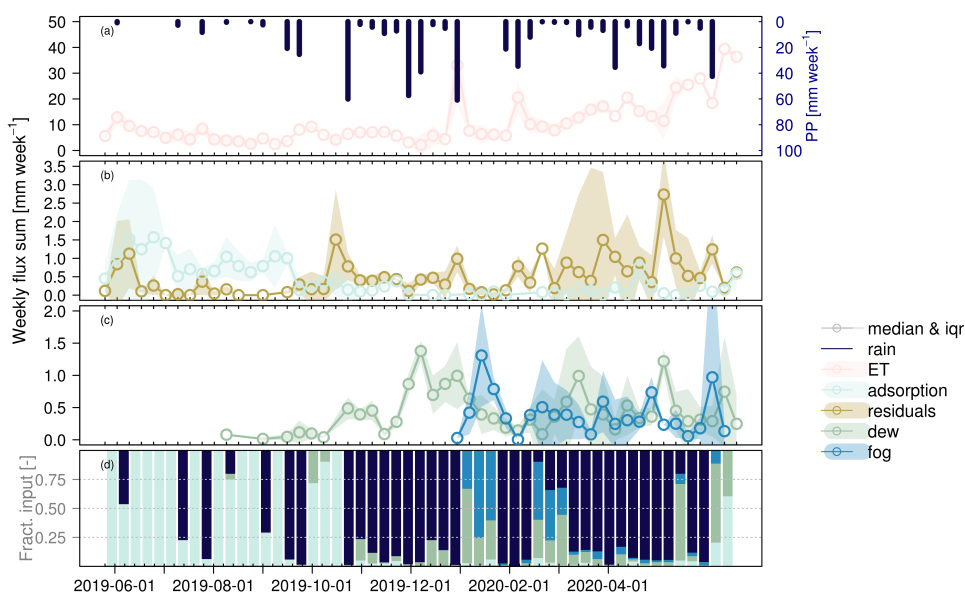
Figure 3. Means of weekly sums across lysimeter columns for (a) ET and rain, (b) adsorption and noise, (c) dew and fog, and (d) relative contributions of rain and NRWIs to total water input per week, respectively. Shading indicates the variability across lysimeter columns expressed as an inter-quartile range (IQR).
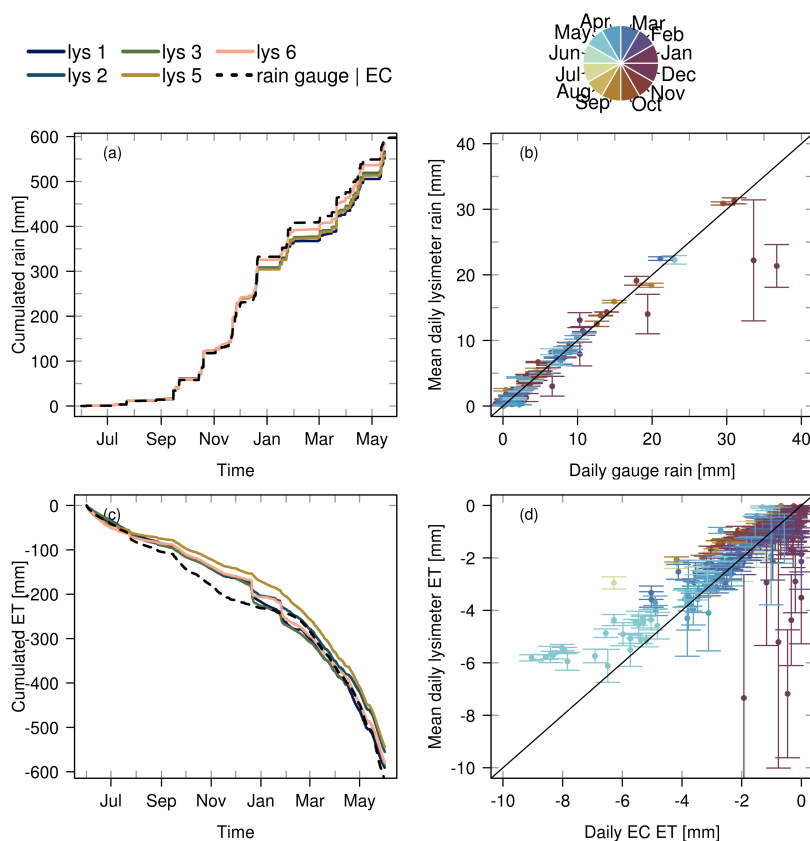
Figure 4. Comparison between cumulative (a,c) and mean diel (b,d) observations of rain and ET between lysimeter and rain gauge (top) and lysimeter and EC (bottom). The points and vertical error bars indicate mean and standard deviation between lysimeter columns, which include measurement uncertainty and spatial variability.

3.2 Water flux sums and their consistency with measurements and theory

The cumulative measured rain is 565.0 ± 11 mm as an average across the six lysimeters. Thereby, the difference between the maximum and minimum across the lysimeters is 30.7 mm, which is an absolute deviation of 5% between columns. For comparison, the rain gauge recorded 597 mm of rain during the same time period. The underestimation of the estimates from lysimeters compared to the rain gauge, as well as the deviation between columns, is mainly caused by a few large rain events in January 2020 (Fig. 4a). The cumulative measured ET across lysimeters is -570.7 ± 20 mm. The annual cumulated difference between lysimeters is 46.7 mm. Annual cumulative ET determined through EC measurements is -619 mm. As in the case of rain, the ET estimates deviate strongest in winter which indicates a technical problem during days with rain at this time of the year, while estimates are more consistent during the rest of the study period (Fig. 4d).

Descriptive statistics of the annual sums of NRWIs across lysimeter columns are summarised in Table 1. The average annual NRWI sum amounted to 42.0 mm with individual contributions of 6.6 mm from fog, 14.1 mm from dew, and 21.2 mm from

Table 1. Mean, median, inter quartile range (IQR) and minimum, and maximum annual sum of individual NRWI fluxes across lysimeter columns. All values are reported in $\mathrm{mm\,year^{-1}}$.

Flux	Mean	Median	IQR	min	max
Fog	6.6	7.6	3.9	3.1	9.5
Dew	14.1	11.8	8.6	9.5	20.2
Adsorption	21.2	16.6	8.3	14.4	34.5
Residuals	*23.7*	*21.2*	*7.6*	*12.8*	*37.3*

Table 2. Uncertainty related to the flux partitioning parameters. The table summarises the annual mean and median fluxes of all lysimeters across all combinations of parameters in the given ranges. Additionally, their interquartile range (IQR) is provided.

Flux	Parameter range	Mean [mm]	Median [mm]	IQR [mm]
Fog	[95, 100] %	6.7	6.7	10.4
Dew	[-2, 0] °C	9.4	8.0	7.1
Adsorption	no perturbation	24.2	22.8	5.3
Residuals	-	25.3	25.2	3.6

adsorption. The differences in flux sums across lysimeters for all NRWI are relatively larger than for rain and ET, with

265 coefficients of variation around $40\,\%$. The largest relative annual deviation between columns was found for adsorption with a difference of $20.0\,\mathrm{mm}$. But the flux which is most affected by the threshold parameter in the lysimeter flux partitioning is fog, which can be seen in Table 2. The IQR for the fluxes decreases the later in the partitioning scheme the respective flux is estimated (Fig. 1). Thereby, for dew and adsorption, the spatial variability between lysimeter columns (IQR in Table 1) exceeds the range of uncertainty related to the partitioning parameters (IQR in Table 2).

270 To assess whether the thermodynamic requirements for dew and adsorption are met at our site we compare the lysimeter-inferred observations of dew and adsorption with their potential occurrence determined with the models from PM, equilibrium evaporation, and the aerodynamic diffusion equation (Fig. 5). Our results show that the measured fluxes are temporally consistent with model results, both concerning diurnal and seasonal dynamics.

In general, the Majadas site has suitable conditions for dew between October 2019 and end of May 2020, from sunset to

275 sunrise. The statistical metrics for the comparison of daily dew duration between lysimeters and models are summarized in Table A2. They show that overall, the models suggest a longer duration of dew conditions by $3\,\mathrm{h\,day^{-1}}$ to $5\,\mathrm{h\,day^{-1}}$. Model statistics from PM and the evaporation model are not deviating from each other indicating that in our application, no difference between the simplified and full PM model is detectable. In the case of adsorption the lysimeter-based estimates agree better with the model predictions (Table A2). When comparing only measurements where at least two out of the five lysimeters show

280 weight increases assigned to adsorption, evaluation statistics improve by one hour. In addition, the agreement of lysimeters is overall stronger during adsorption than during dew conditions (Fig. 5). Single lysimeters, however, frequently also measured adsorption until midday and before sunset.
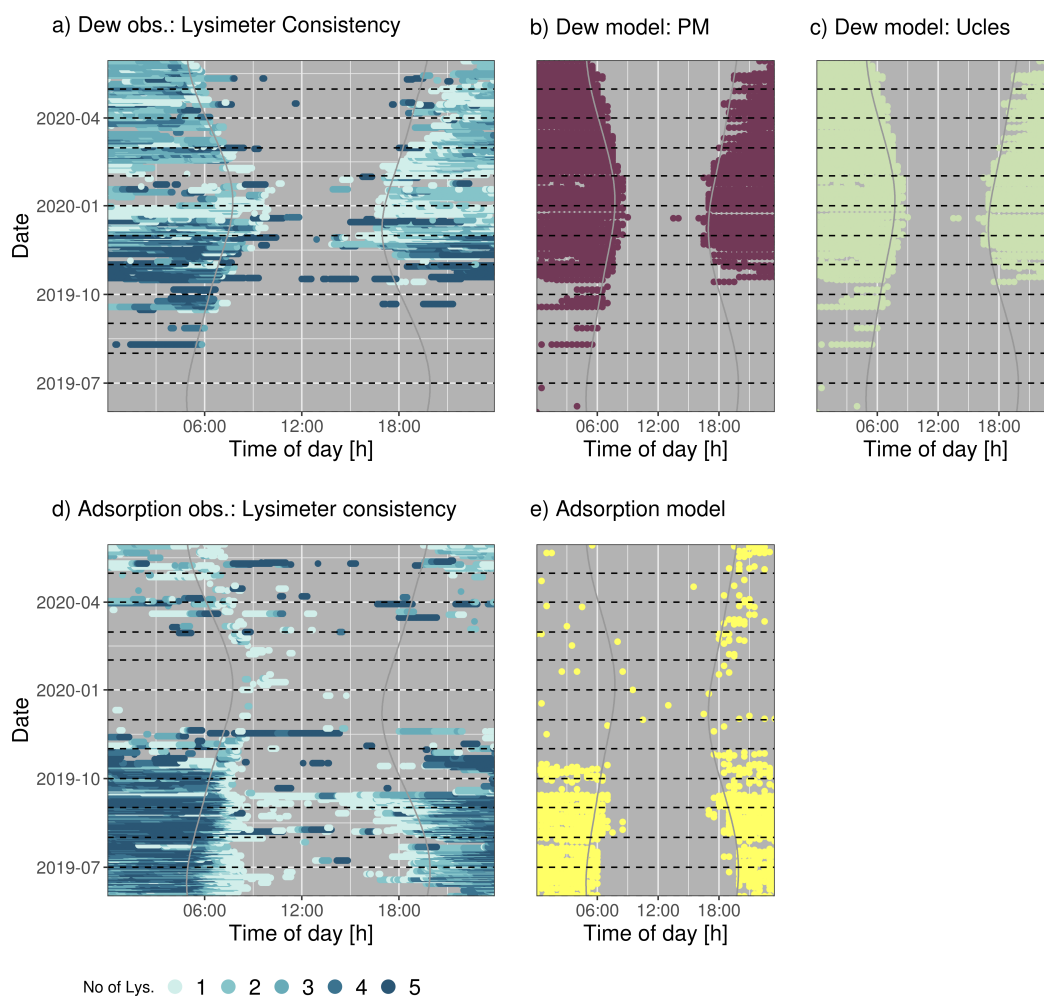
Figure 5. Diel and seasonal dynamics of consistency of inferred a) dew and d) adsorption, across all lysimeters. Modeled occurrence is presented for dew from b) Penman-Monteith model (PM), c) equilibrium evaporation model, and for adsorption using d) the aerodynamic diffusion equation. Solid lines mark sunrise and sunset, determined by the geographic coordinates of the site.

4 Discussion

In this study, we showed that large weighing lysimeters and a few ancillary measurements can be used to efficiently disentangle
285 and therefore quantify all types of surface water fluxes, particularly NRWI. Our data from a semi-arid Mediterranean savanna
site shows that the climatic conditions fulfill the thermodynamic requirements to induce diel cycles of evaporation and conden-
sation at almost all times of the year. The routine proposed to detect and distinguish NRWI is successfully validated against
models based on energy balance and moisture gradients, regarding the occurrence of the process.

We found that NRWIs occur frequently at our site, in line with previous research in such a climate regime. The occurrence
of both adsorption and dew was shown by Zhang et al. (2019b). We support their observation that dew formation and ad-
sorption dominate at different times of the year. Regular dew formation ($120\,\mathrm{nights\,year^{-1}}$ to $200\,\mathrm{nights\,year^{-1}}$) has been
reported across sites (Tomaszkiewicz et al., 2015). In a similar semi-arid steppe ecosystem in Spain, the mean number of
days per year with suitable conditions for dew formation was $285\,\mathrm{days}$ (Uclés et al., 2014), however, their ecosystem is close
to the Mediterranean sea and likely, therefore, receives more humidity than Majadas. Our observation that especially nights
are prone to the formation of NRWI is also documented in the literature. Dew formation length has often been reported to
correlate with the length of the night (Tomaszkiewicz et al., 2015) and was in another Spanish site reported to last on average
$9.3 \pm 3.2\,\mathrm{hours\,night^{-1}}$ (Uclés et al., 2014). In contrast, for adsorption, reported observation times differ. Kosmas et al. (1998)
observed the flux to occur mainly between 0:00 and 6:00 h and also Saaltink et al. (2020) found suitable night-time conditions
for adsorption through a reversed gradient of vapor concentration between soil and atmosphere from lysimeter observations and
confirmed it with a fully coupled numerical model. Yet, Verhoef et al. (2006) found adsorption occurring during the afternoon
and ceasing at night. Since changes in T_s and their effects on the phase equilibrium of water are one of the main controlling
factors of adsorption, the different findings between studies could be related to site-specific timing of surface exposure to
radiation.

Next to the diagnosed occurrences, also the NRWI amounts we determined are within the range of previously reported
estimates for similar climate regimes. At our study site Majadas, the largest annual NRWI contribution is adsorption with
$21.2\,\mathrm{mm\,year^{-1}}$. This value is relatively low, compared to sites close to the sea, where values of $81\,\mathrm{mm\,year^{-1}}$ (Saaltink
et al., 2020), and $26\,\mathrm{mm}$ to $110\,\mathrm{mm}$ between April and October have been reported (Kosmas et al., 2001). But it matches well
with observations from Qubaja et al. (2020) that measured annual adsorption of $14\,\mathrm{mm\,year^{-1}}$ using flux chambers in a semi-
arid pine forest in Israel. Furthermore, dew and fog quantified here at $14.4\,\mathrm{mm\,year^{-1}}$ and $6.6\,\mathrm{mm\,year^{-1}}$, respectively, are
within the range reported from other sites which are depending on site $4\,\mathrm{mm\,year^{-1}}$ to $39\,\mathrm{mm\,year^{-1}}$ for dew (Tomaszkiewicz
et al., 2015) and $1.3\,\mathrm{mm\,year^{-1}}$ to $50\,\mathrm{mm\,year^{-1}}$ for fog (Zhang et al., 2019b; Kidron and Starinsky, 2019). It is important to
remark, however, that part of the large variability concerning the length of occurrence and condensation rates for NRWI could
be related to biases of the measurement devices. Micro lysimeters, until now one of the most widely used instruments, were
reported by Kidron and Kronenfeld (2020b) to overestimate NRWI likely due to greater heat loss through the walls, compared
to the surrounding unperturbed soil.

We found differences in the absolute annual NRWI sums between individual lysimeters that can be attributed either to (i)
spatial variability (heterogeneity) in the soil and vegetation characteristics affecting the energy balance, or (ii) instrumental
and methodological uncertainty. Particularly for the latter, external disturbances by wind or animals and internal disturbances
such as data gaps, and data processing have been shown to alter results significantly (Schrader et al., 2013; Nolz et al., 2013).
Developing processing routines for raw data from large weighing lysimeters has challenged researchers during the last decade
(Schrader et al., 2013; Peters et al., 2014, 2016, 2017; Hannes et al., 2015). To assess the robustness of the processing we
compared rain across lysimeters as rain is expected to be similar across nearby lysimeters and heterogeneous soils and vege-
tation. The variation of rain across lysimeters is only $5\,\%$, which is of a similar magnitude reported in other studies (Hannes

et al., 2015; Schneider et al., 2021). Model simulations independently confirmed, that the conditions at night are suitable for
NRWI, although especially for dew the simulations showed that the potential for dew formation is generally longer than actual
occurrence, measured with lysimeters.

A focus of this study was partitioning the lysimeter ΔW into water flux classes. This approach includes the simplified
assumption that one flux is always dominating over the others at each time step. In reality, the fluxes can occur simultaneously
with their relative importance shifting gradually over time (Li et al., 2021b), but postulate to be minimal at the time scale we are
looking at. Ideally, we would account for a statistical probability ratio between different NRWI per time interval. But current
research that is quantifying such ratios is too scarce for generalization (Li et al., 2021b).

Disentangling individual NRWI fluxes is nevertheless important because of different respective i) controlling factors and
ii) implications for the ecosystem. Better knowledge on controlling factors can help to identify potential NRWI occurrence
also in ecosystems without specialized measurement devices. The role of dew has often been reported as moistening plant
surfaces with direct leaf water uptake (Tomaszkiewicz et al., 2015). Soil vapor adsorption, however, occurs at low Ψ where
grasses in Majadas have already senesced. Nevertheless, due to it's continuous occurrence in periods of low SWC, it would
be a beneficial ecological strategy for organisms to use this diel water input. So far, it is recognized that microbial and lichen
respiration is triggered by adsorption (Evans et al., 2019; McHugh et al., 2015; Dirks et al., 2010; Li et al., 2021a; Gliksman
et al., 2017) but more research is necessary to understand the impact of this flux on different organisms. The approach applied
most frequently in the literature as well as in this study is based on a discontinuous tree-based classification system which was
implemented similarly as suggested by Zhang et al. (2019a). As an extension of their system one node was added to account for
prior knowledge on the controls of adsorption. The prior knowledge for soil adsorption stems, however, from smaller samples
at equilibrium conditions in the laboratory (Arthur et al., 2016). Our application to point measurements of rH and SWC
from above and below the soil surface assumes that by choosing the statistical upper envelope we can distinguish equilibrium
conditions from remaining noise in the time series as best as possible. Although uncertainty remains about the real shape of
this relationship, this approach gives a more conservative estimate of the adsorption amount and helps prevent overestimation.
The validity of this relationship is further confirmed by having a similar shape independently whether it was derived from the
periods when lysimeter measurements unanimously were classified as adsorption (before including residuals as a final node)
or deduced from negative EC derived λE.

The advantage of the discontinuous tree-based classification is that it is applicable widely because the necessary data is
commonly measured. The disadvantage is that selection of the parameters and thresholds in the classification algorithm is
critical, especially at the upper nodes, where choices propagate into the estimates of flux classes of deeper nodes. Our test
on different parameter combinations found that the strongest impact on flux quantity was for fog, followed by adsorption.
Nevertheless, the ranking was not affected by choice of parameters and thresholds, e.g. in all tested cases adsorption had the
largest contribution to annual flux sums.

Apart from instrumental and methodological uncertainty, the spatial heterogeneity of soil and vegetation characteristics of
the field site (Nair et al., 2019) can affect our results. In fact, dew and adsorption amounts are both reported to vary substantially
with the surface cover type (Uclés et al., 2016), soil exposure (Kosmas et al., 2001), shading hours (Uclés et al., 2015), distance

from trees (Verhoef et al., 2006; Qubaja et al., 2020) and soil texture, particularly clay and sand content (Kosmas et al.,
360 2001; Orchiston, 1952; Yamanaka and Yonetani, 1999). Verhoef et al. (2006) showed in a measurement campaign with eight
lysimeters concentrically arranged around a single oak tree that at the most exposed spots adsorption was doubled compared
to the shaded spot. At our site, there are also individual sparse trees (Bogdanovich et al., 2021) which cause small-scale
differences in shading. Since some lysimeter columns are more exposed than others, part of the deviation in NRWI could be
explained by spatial heterogeneity. This is supported by measurements of soil Ψ within the individual columns, which showed
365 that one column had an overall greater mean T_{soil} in summer and the threshold of potential adsorption conditions was reached
nearly a full month earlier than in other columns. Micrometeorological variables were however not measured individually at
each column and therefore we have no insight into the exact causes of spatial heterogeneity in dew formation. The applied
models both only suggest times of dew formation potential based on measurements at the central facility, while the quantity is
derived from weight changes. For the same reason, spatial differences are robust and follow-up investigations can be targeted
370 towards understanding their causes.

Notably, the current study also provides an opportunity to propose a way forward in adsorption research based on the ob-
served similar temporal pattern between negative EC derived λE and lysimeter vapor adsorption occurrence. EC instruments
are currently one of the most popular instruments to estimate λE at an ecosystem scale (Baldocchi, 2014, 2020). But measure-
ments are frequently discarded when the underlying micrometeorological assumptions of the technology are not met (Göckede
375 et al., 2004). This often affects night-time EC measurements (Massman and Lee, 2002). Previous research in a pine forest in
Israel also indicated that EC-derived λE tends to be negative at night during adsorption (Qubaja et al., 2020). At our site, this
pattern is obvious and indicates that night-time EC measurements could serve to detect adsorption (Fig. 6).

To help assess the relevance of adsorption, we suggest revaluing night-time λE fluxes of EC instruments. This could also
help to up scaling and in doing so overcoming the problems with clarifying the role of NRWI across research communities
380 (Gerlein-Safdi, 2021), for example concerning energy balance closure of EC (de Roode et al., 2010), ecological significance of
foliar water uptake (Berry et al., 2019) and impacts on remote sensing products (Xu et al., 2021). Irrespectively, our findings
underline the necessity for methods on processes of the water cycle during the night to avoid biased measurements towards
evaporation while missing condensation.

5 Conclusions and outlook

385 In this manuscript, we derive NRWI from time series of automated weighted lysimeters and compare their length of occurrence
with established model estimations. In summary, our data suggest that this semi-arid savanna ecosystem switches between
evaporation and condensation almost daily. Attributing the condensation pattern into different NRWI sheds light on the distinct
mechanisms that are each dominant in a different season. In summer, adsorption of atmospheric vapor on soil particles is
facilitated by large diel temperature differences and dry soils lead to steep gradients of atmospheric vapor pressure between the
390 atmosphere and the soil air driving vapor diffusion. In winter and spring, high rH leads to frequent fog deposition and surface
cooling to dew condensation. Spatial heterogeneity of vegetation, soil characteristics, and radiation regimes, together with
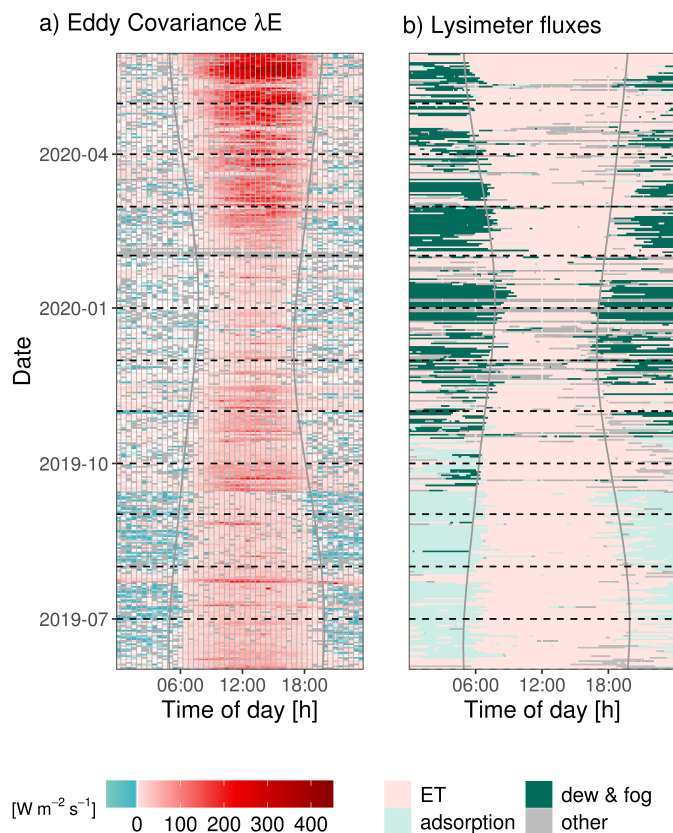
Figure 6. Diel and seasonal variation of a) quality filtered λE fluxes from EC and b) assigned lysimeter fluxes. Solid curved vertical lines mark sunrise and sunset, respectively, determined with the geographic coordinates of the field site.

measurement uncertainties are stronger reflected in NRWI than in other fluxes of surface water exchange. Although between 01.06.2019 and 31.05.2020, the total NRWI sum comprises only 7.4% of the local water input, the relative contribution strongly varies weekly. Rain frequency is unevenly distributed within the year and especially atmospheric adsorption stands

395 out as the only water input during 11 weeks in the dry season. The ecological relevance of this flux has yet to be scrutinized.

Our analysis focuses on lysimeters, that cover only a spatial area of $1\,\mathrm{m}^2$, each. We show that the temporal variability of the NRWI derived from the instruments is coherent with negative LE fluxes at dry conditions. Based on this observation, future work could focus on revalue night-time λE fluxes from EC instruments to improve the spatial representativeness and assess the relevance of NRWI at the larger scale and across seasonally dry ecosystems.

Code and data availability. The raw and processed lysimeter data used in this study, as well as the meteorological and radiometric variables necessary for partitioning the water fluxes will be made publicly available after the manuscript is accepted in a Zenodo repository together with the full code for the lysimeter raw weight processing and partitioning in R statistical programming language. The code and data for the modeling can be provided on request.

Author contributions. MM, RO, MR, OPP, SP designed the setup and planned the study. OK, GM, AC, TEM, MM, and OPP were maintaining the site and instrumentation and conducted the measurements. SP, TEM, and TW processed the data. SP analyzed the data and prepared the original draft, both under the supervision of MM, RO, TEM, and AH. All authors discussed, reviewed and edited the manuscript.

Competing interests. The authors declare that they have no conflict of interest.

Acknowledgements. SP acknowledge the support for this research through the International Max Planck Research School for Global Biogeochemical Cycles (IMPRS-gBGC) at the University of Jena. The authors acknowledge the Alexander von Humboldt Foundation for supporting this research through the Max Planck Research Prize 2013 to Markus Reichstein. RO was supported by funding from the German Research Foundation (Emmy Noether Grant 391059971). We thank the city council of Majadas de Tietar for support. Our thanks go to Martin Strube, Ramón López-Jimenez, Martin Hertel, and the Freiland group at the MPI-BGC for great technical and scientific assistance during fieldwork. SP would further like to thank Andre Peters and Johanna Blöcher for their helpful comments and suggestions.

References

415   Agam, N. and Berliner, P.: Dew formation and water vapor adsorption in semi-arid environments—A review, Journal of Arid Environments, 65, 572–590, https://doi.org/10.1016/j.jaridenv.2005.09.004, https://linkinghub.elsevier.com/retrieve/pii/S0140196305002235, 2006.

Aguirre-Gutiérrez, C. A., Holwerda, F., Goldsmith, G. R., Delgado, J., Yepez, E., Carbajal, N., Escoto-Rodríguez, M., and Arredondo, J. T.: The importance of dew in the water balance of a continental semiarid grassland, Journal of Arid Environments, 168, 26–35, https://doi.org/10.1016/j.jaridenv.2019.05.003, https://linkinghub.elsevier.com/retrieve/pii/S0140196319300643, 2019.

420   Aparecido, L. M. T., Miller, G. R., Cahill, A. T., and Moore, G. W.: Leaf surface traits and water storage retention affect photosynthetic responses to leaf surface wetness among wet tropical forest and semiarid savanna plants, Tree Physiology, 37, 1285–1300, https://doi.org/10.1093/treephys/tpx092, http://academic.oup.com/treephys/article/37/10/1285/3977790, 2017.

Arthur, E., Tuller, M., Moldrup, P., and de Jonge, L. W.: Evaluation of theoretical and empirical water vapor sorption isotherm models for soils, Water Resources Research, 52, 190–205, https://doi.org/10.1002/2015WR017681, https://onlinelibrary.wiley.com/doi/abs/10.1002/2015WR017681, 2016.

425

Baldocchi, D.: Measuring fluxes of trace gases and energy between ecosystems and the atmosphere - the state and future of the eddy covariance method, Global Change Biology, 20, 3600–3609, https://doi.org/10.1111/gcb.12649, http://doi.wiley.com/10.1111/gcb.12649, 2014.

Baldocchi, D. D.: How eddy covariance flux measurements have contributed to our understanding of Global Change Biology, Global Change

430   Biology, 26, 242–260, https://doi.org/10.1111/gcb.14807, https://onlinelibrary.wiley.com/doi/10.1111/gcb.14807, 2020.

Ben-Asher, J., Alpert, P., and Ben-Zvi, A.: Dew is a major factor affecting vegetation water use efficiency rather than a source of water in the eastern Mediterranean area, Water Resources Research, 46, 2008WR007 484, https://doi.org/10.1029/2008WR007484, https://onlinelibrary.wiley.com/doi/abs/10.1029/2008WR007484, 2010.

Berry, Z. C., White, J. C., and Smith, W. K.: Foliar uptake, carbon fluxes and water status are affected by the timing of daily fog in

435   saplings from a threatened cloud forest, Tree Physiology, 34, 459–470, https://doi.org/10.1093/treephys/tpu032, https://academic.oup.com/treephys/article-lookup/doi/10.1093/treephys/tpu032, 2014.

Berry, Z. C., Emery, N. C., Gotsch, S. G., and Goldsmith, G. R.: Foliar water uptake: Processes, pathways, and integration into plant water budgets: Foliar Water Uptake, Plant, Cell & Environment, 42, 410–423, https://doi.org/10.1111/pce.13439, http://doi.wiley.com/10.1111/pce.13439, 2019.

440   Bogdanovich, E., Perez-Priego, O., El-Madany, T. S., Guderle, M., Pacheco-Labrador, J., Levick, S. R., Moreno, G., Carrara, A., Pilar Martín, M., and Migliavacca, M.: Using terrestrial laser scanning for characterizing tree structural parameters and their changes under different management in a Mediterranean open woodland, Forest Ecology and Management, 486, 118 945, https://doi.org/10.1016/j.foreco.2021.118945, https://linkinghub.elsevier.com/retrieve/pii/S0378112721000347, 2021.

Camuffo, D.: Condensation-evaporation cycles in pore and capillary systems according to the Kelvin model, Water, Air, and Soil Pollution,

445   21, 151–159, https://doi.org/10.1007/BF00163620, http://link.springer.com/10.1007/BF00163620, 1984.

Dawson, T. E. and Goldsmith, G. R.: The value of wet leaves, New Phytologist, 219, 1156–1169, https://doi.org/10.1111/nph.15307, http://doi.wiley.com/10.1111/nph.15307, 2018.

de Roode, S. R., Bosveld, F. C., and Kroon, P. S.: Dew Formation, Eddy-Correlation Latent Heat Fluxes, and the Surface Energy Imbalance at Cabauw During Stable Conditions, Boundary-Layer Meteorology, 135, 369–383, https://doi.org/10.1007/s10546-010-9476-1, http://link.

450   springer.com/10.1007/s10546-010-9476-1, 2010.

Dijkema, J., Koonce, J., Shillito, R., Ghezzehei, T., Berli, M., van der Ploeg, M., and van Genuchten, M.: Water Distribution in an Arid Zone Soil: Numerical Analysis of Data from a Large Weighing Lysimeter, Vadose Zone Journal, 17, 0, https://doi.org/10.2136/vzj2017.01.0035, https://dl.sciencesocieties.org/publications/vzj/abstracts/17/1/170035, 2018.

Dirks, I., Navon, Y., Kanas, D., Dumbur, R., and Grünzweig, J. M.: Atmospheric water vapor as driver of litter decomposition in Mediterranean shrubland and grassland during rainless seasons: WATER VAPOR AS DRIVER OF LITTER DECOMPOSITION, Global Change Biology, 16, 2799–2812, https://doi.org/10.1111/j.1365-2486.2010.02172.x, http://doi.wiley.com/10.1111/j.1365-2486.2010.02172.x, 2010.

Duvdevani, S.: Dew in Israel and its effect on plants, 1963.

Edlefsen, N., Anderson, A., et al.: Thermodynamics of soil moisture, Hilgardia, 15, 31–298, 1943.

El-Madany, T. S., Reichstein, M., Perez-Priego, O., Carrara, A., Moreno, G., Pilar Martín, M., Pacheco-Labrador, J., Wohlfahrt, G., Nieto, H., Weber, U., Kolle, O., Luo, Y.-P., Carvalhais, N., and Migliavacca, M.: Drivers of spatio-temporal variability of carbon dioxide and energy fluxes in a Mediterranean savanna ecosystem, Agricultural and Forest Meteorology, 262, 258–278, https://doi.org/10.1016/j.agrformet.2018.07.010, https://linkinghub.elsevier.com/retrieve/pii/S0168192318302314, 2018.

El-Madany, T. S., Carrara, A., Martín, M. P., Moreno, G., Kolle, O., Pacheco-Labrador, J., Weber, U., Wutzler, T., Reichstein, M., and Migliavacca, M.: Drought and heatwave impacts on semi-arid ecosystems' carbon fluxes along a precipitation gradient, Philosophical Transactions of the Royal Society B: Biological Sciences, 375, 20190 519, https://doi.org/10.1098/rstb.2019.0519, https://royalsocietypublishing.org/doi/10.1098/rstb.2019.0519, 2020.

El-Madany, T. S., Reichstein, M., Carrara, A., Martín, M. P., Moreno, G., Gonzalez-Cascon, R., Peñuelas, J., Ellsworth, D. S., Burchard-Levine, V., Hammer, T. W., Knauer, J., Kolle, O., Luo, Y., Pacheco-Labrador, J., Nelson, J. A., Perez-Priego, O., Rolo, V., Wutzler, T., and Migliavacca, M.: How Nitrogen and Phosphorus Availability Change Water Use Efficiency in a Mediterranean Savanna Ecosystem, Journal of Geophysical Research: Biogeosciences, 126, https://doi.org/10.1029/2020JG006005, https://onlinelibrary.wiley.com/doi/10.1029/2020JG006005, 2021.

Evans, S., Todd-Brown, K. E. O., Jacobson, K., and Jacobson, P.: Non-rainfall Moisture: A Key Driver of Microbial Respiration from Standing Litter in Arid, Semiarid, and Mesic Grasslands, Ecosystems, https://doi.org/10.1007/s10021-019-00461-y, http://link.springer.com/10.1007/s10021-019-00461-y, 2019.

Feigenwinter, C., Franceschi, J., Larsen, J. A., Spirig, R., and Vogt, R.: On the performance of microlysimeters to measure non-rainfall water input in a hyper-arid environment with focus on fog contribution, Journal of Arid Environments, 182, 104 260, https://doi.org/10.1016/j.jaridenv.2020.104260, https://linkinghub.elsevier.com/retrieve/pii/S0140196320301592, 2020.

Gerlein-Safdi, C., Gauthier, P. P. G., and Caylor, K. K.: Dew-induced transpiration suppression impacts the water and isotope balances of Colocasia leaves, Oecologia, 187, 1041–1051, https://doi.org/10.1007/s00442-018-4199-y, http://link.springer.com/10.1007/s00442-018-4199-y, 2018.

Gerlein-Safdi, C.: Seeing dew deposition from satellites: leveraging microwave remote sensing for the study of water dynamics in and on plants, New Phytologist, 231, 5–7, https://doi.org/10.1111/nph.17418, https://onlinelibrary.wiley.com/doi/10.1111/nph.17418, 2021.

Gliksman, D., Rey, A., Seligmann, R., Dumbur, R., Sperling, O., Navon, Y., Haenel, S., De Angelis, P., Arnone, J. A., and Grünzweig, J. M.: Biotic degradation at night, abiotic degradation at day: positive feedbacks on litter decomposition in drylands, Global Change Biology, 23, 1564–1574, https://doi.org/10.1111/gcb.13465, https://onlinelibrary.wiley.com/doi/10.1111/gcb.13465, 2017.

Groh, J., Vanderborght, J., Pütz, T., and Vereecken, H.: How to Control the Lysimeter Bottom Boundary to Investigate the Effect of Climate Change on Soil Processes?, Vadose Zone Journal, 15, vzj2015.08.0113, https://doi.org/10.2136/vzj2015.08.0113, http://doi.wiley.com/10.2136/vzj2015.08.0113, 2016.

Groh, J., Slawitsch, V., Herndl, M., Graf, A., Vereecken, H., and Pütz, T.: Determining dew and hoar frost formation for a low mountain range and alpine grassland site by weighable lysimeter, Journal of Hydrology, 563, 372–381, https://doi.org/10.1016/j.jhydrol.2018.06.009, https://linkinghub.elsevier.com/retrieve/pii/S0022169418304153, 2018.

Göckede, M., Rebmann, C., and Foken, T.: A combination of quality assessment tools for eddy covariance measurements with footprint modelling for the characterisation of complex sites, Agricultural and Forest Meteorology, 127, 175–188, https://doi.org/10.1016/j.agrformet.2004.07.012, https://linkinghub.elsevier.com/retrieve/pii/S016819230400200X, 2004.

Hannes, M., Wollschläger, U., Schrader, F., Durner, W., Gebler, S., Pütz, T., Fank, J., von Unold, G., and Vogel, H.-J.: A comprehensive filtering scheme for high-resolution estimation of the water balance components from high-precision lysimeters, Hydrology and Earth System Sciences, 19, 3405–3418, https://doi.org/10.5194/hess-19-3405-2015, https://www.hydrol-earth-syst-sci.net/19/3405/2015/, 2015.

IUSS Working Group WRB: Working Group WRB (2015) World reference base for soil resources 2014, update 2015, International soil classification system for naming soils and creating legends for soil maps. World Soil Resources Reports, 2015.

Jacobs, A. F. G., Heusinkveld, B. G., Wichink Kruit, R. J., and Berkowicz, S. M.: Contribution of dew to the water budget of a grassland area in the Netherlands, Water Resources Research, 42, https://doi.org/10.1029/2005WR004055, http://doi.wiley.com/10.1029/2005WR004055, 2006.

Jung, M., Reichstein, M., Ciais, P., Seneviratne, S. I., Sheffield, J., Goulden, M. L., Bonan, G., Cescatti, A., Chen, J., de Jeu, R., Dolman, A. J., Eugster, W., Gerten, D., Gianelle, D., Gobron, N., Heinke, J., Kimball, J., Law, B. E., Montagnani, L., Mu, Q., Mueller, B., Oleson, K., Papale, D., Richardson, A. D., Roupsard, O., Running, S., Tomelleri, E., Viovy, N., Weber, U., Williams, C., Wood, E., Zaehle, S., and Zhang, K.: Recent decline in the global land evapotranspiration trend due to limited moisture supply, Nature, 467, 951–954, https://doi.org/10.1038/nature09396, http://www.nature.com/articles/nature09396, 2010.

Jung, M., Schwalm, C., Migliavacca, M., Walther, S., Camps-Valls, G., Koirala, S., Anthoni, P., Besnard, S., Bodesheim, P., Carvalhais, N., Chevallier, F., Gans, F., Goll, D. S., Haverd, V., Köhler, P., Ichii, K., Jain, A. K., Liu, J., Lombardozzi, D., Nabel, J. E. M. S., Nelson, J. A., O'Sullivan, M., Pallandt, M., Papale, D., Peters, W., Pongratz, J., Rödenbeck, C., Sitch, S., Tramontana, G., Walker, A., Weber, U., and Reichstein, M.: Scaling carbon fluxes from eddy covariance sites to globe: synthesis and evaluation of the FLUXCOM approach, Biogeosciences, 17, 1343–1365, https://doi.org/10.5194/bg-17-1343-2020, https://www.biogeosciences.net/17/1343/2020/, 2020.

Kidron, G. J. and Kronenfeld, R.: Atmospheric humidity is unlikely to serve as an important water source for crustose soil lichens in the Tabernas Desert, Journal of Hydrology and Hydromechanics, 68, 359–367, https://doi.org/10.2478/johh-2020-0034, https://content.sciendo.com/view/journals/johh/68/4/article-p359.xml, 2020a.

Kidron, G. J. and Kronenfeld, R.: Microlysimeters overestimate the amount of non-rainfall water – an experimental approach, CATENA, 194, 104 691, https://doi.org/10.1016/j.catena.2020.104691, https://linkinghub.elsevier.com/retrieve/pii/S0341816220302411, 2020b.

Kidron, G. J. and Starinsky, A.: Measurements and ecological implications of non-rainfall water in desert ecosystems—A review, Ecohydrology, 12, https://doi.org/10.1002/eco.2121, https://onlinelibrary.wiley.com/doi/abs/10.1002/eco.2121, 2019.

Kohfahl, C., Molano-Leno, L., Martínez, G., Vanderlinden, K., Guardiola-Albert, C., and Moreno, L.: Determining groundwater recharge and vapor flow in dune sediments using a weighable precision meteo lysimeter, Science of The Total Environment, 656, 550–557, https://doi.org/10.1016/j.scitotenv.2018.11.415, https://linkinghub.elsevier.com/retrieve/pii/S0048969718347703, 2019.

Kosmas, C., Danalatos, N., Poesen, J., and van Wesemael, B.: The effect of water vapour adsorption on soil moisture content under Mediterranean climatic conditions, Agricultural Water Management, 36, 157–168, https://doi.org/10.1016/S0378-3774(97)00050-4, https://linkinghub.elsevier.com/retrieve/pii/S0378377497000504, 1998.

Kosmas, C., Marathianou, M., Gerontidis, S., Detsis, V., Tsara, M., and Poesen, J.: Parameters affecting water vapor adsorption by the soil under semi-arid climatic conditions, Agricultural Water Management, p. 18, 2001.

Li, S., Xiao, B., Sun, F., and Kidron, G. J.: Moss-dominated biocrusts enhance water vapor sorption capacity of surface soil and increase non-rainfall water deposition in drylands, Geoderma, 388, 114 930, https://doi.org/10.1016/j.geoderma.2021.114930, https://linkinghub.elsevier.com/retrieve/pii/S0016706121000045, 2021a.

Li, Y., Aemisegger, F., Riedl, A., Buchmann, N., and Eugster, W.: The role of dew and radiation fog inputs in the local water cycling of a temperate grassland during dry spells in central Europe, Hydrology and Earth System Sciences, 25, 2617–2648, https://doi.org/10.5194/hess-25-2617-2021, https://hess.copernicus.org/articles/25/2617/2021/, 2021b.

Luo, Y., El-Madany, T. S., Filippa, G., Ma, X., Ahrens, B., Carrara, A., Gonzalez-Cascon, R., Cremonese, E., Galvagno, M., Hammer, T. W., Pacheco-Labrador, J., Martín, M. P., Moreno, G., Perez-Priego, O., Reichstein, M., Richardson, A. D., Römermann, C., and Migliavacca, M.: Using Near-Infrared-Enabled Digital Repeat Photography to Track Structural and Physiological Phenology in Mediterranean Tree–Grass Ecosystems, Remote Sensing, 10, 1293, https://doi.org/10.3390/rs10081293, http://www.mdpi.com/2072-4292/10/8/1293, 2018.

Luo, Y., El-Madany, T., Ma, X., Nair, R., Jung, M., Weber, U., Filippa, G., Bucher, S. F., Moreno, G., Cremonese, E., Carrara, A., Gonzalez-Cascon, R., Cáceres Escudero, Y., Galvagno, M., Pacheco-Labrador, J., Martín, M. P., Perez-Priego, O., Reichstein, M., Richardson, A. D., Menzel, A., Römermann, C., and Migliavacca, M.: Nutrients and water availability constrain the seasonality of vegetation activity in a Mediterranean ecosystem, Global Change Biology, 26, 4379–4400, https://doi.org/10.1111/gcb.15138, https://onlinelibrary.wiley.com/doi/abs/10.1111/gcb.15138, 2020.

Massman, W. and Lee, X.: Eddy covariance flux corrections and uncertainties in long-term studies of carbon and energy exchanges, Agricultural and Forest Meteorology, 113, 121–144, https://doi.org/10.1016/S0168-1923(02)00105-3, https://linkinghub.elsevier.com/retrieve/pii/S0168192302001053, 2002.

McHugh, T. A., Morrissey, E. M., Reed, S. C., Hungate, B. A., and Schwartz, E.: Water from air: an overlooked source of moisture in arid and semiarid regions, Scientific Reports, 5, 13 767, https://doi.org/10.1038/srep13767, http://www.nature.com/articles/srep13767, 2015.

Meissner, R., Rupp, H., and Schubert, M.: Novel lysimeter techniques — a basis for the improved investigation of water, gas, and solute transport in soils, p. 6.

Migliavacca, M., Perez-Priego, O., Rossini, M., El-Madany, T. S., Moreno, G., van der Tol, C., Rascher, U., Berninger, A., Bessenbacher, V., Burkart, A., Carrara, A., Fava, F., Guan, J.-H., Hammer, T. W., Henkel, K., Juarez-Alcalde, E., Julitta, T., Kolle, O., Martín, M. P., Musavi, T., Pacheco-Labrador, J., Pérez-Burgueño, A., Wutzler, T., Zaehle, S., and Reichstein, M.: Plant functional traits and canopy structure control the relationship between photosynthetic CO_2 uptake and far-red sun-induced fluorescence in a Mediterranean grassland under different nutrient availability, New Phytologist, 214, 1078–1091, https://doi.org/10.1111/nph.14437, http://doi.wiley.com/10.1111/nph.14437, 2017.

Milly, P.: A simulation analysis of thermal effects on evaporation from soil, Water Resources Research, 20, 1087–1098, 1984.

Monteith, J. L.: Evaporation and environment. The stage and movement of water in living organisms., in: 19th Symp. Soc. Exp. Biol., Cambridge university press, 1965.

Nair, R. K. F., Morris, K. A., Hertel, M., Luo, Y., Moreno, G., Reichstein, M., Schrumpf, M., and Migliavacca, M.: N : P stoichiometry and habitat effects on Mediterranean savanna seasonal root dynamics, Biogeosciences, 16, 1883–1901, https://doi.org/10.5194/bg-16-1883-2019, https://www.biogeosciences.net/16/1883/2019/, 2019.

Nelson, J., Carvalhais, N., Cuntz, M., Delpierre, N., Knauer, J., Ogée, J., Migliavacca, M., Reichstein, M., and Jung, M.: Coupling Water and Carbon Fluxes to Constrain Estimates of Transpiration: The TEA Algorithm, Journal of Geophysical Research: Biogeosciences, 123, 3617–3632, https://doi.org/10.1029/2018JG004727, https://onlinelibrary.wiley.com/doi/abs/10.1029/2018JG004727, 2018.

Nolz, R., Kammerer, G., and Cepuder, P.: Interpretation of lysimeter weighing data affected by wind, Journal of Plant Nutrition and Soil Science, 176, 200–208, https://doi.org/10.1002/jpln.201200342, http://doi.wiley.com/10.1002/jpln.201200342, 2013.

Orchiston, H. D.: Adsorption of water vapor: I. Soils at 25 °C., 1952.

Panwar, A., Kleidon, A., and Renner, M.: Do Surface and Air Temperatures Contain Similar Imprints of Evaporative Conditions?, Geophysical Research Letters, 46, 3802–3809, https://doi.org/10.1029/2019GL082248, https://onlinelibrary.wiley.com/doi/abs/10.1029/2019GL082248, 2019.

Perez-Priego, O., El-Madany, T. S., Migliavacca, M., Kowalski, A. S., Jung, M., Carrara, A., Kolle, O., Martín, M. P., Pacheco-Labrador, J., Moreno, G., and Reichstein, M.: Evaluation of eddy covariance latent heat fluxes with independent lysimeter and sapflow estimates in a Mediterranean savannah ecosystem, Agricultural and Forest Meteorology, 236, 87–99, https://doi.org/10.1016/j.agrformet.2017.01.009, https://linkinghub.elsevier.com/retrieve/pii/S0168192317300096, 2017.

Perez-Priego, O., Katul, G., Reichstein, M., El-Madany, T. S., Ahrens, B., Carrara, A., Scanlon, T. M., and Migliavacca, M.: Partitioning Eddy Covariance Water Flux Components Using Physiological and Micrometeorological Approaches, Journal of Geophysical Research: Biogeosciences, 123, 3353–3370, https://doi.org/10.1029/2018JG004637, http://doi.wiley.com/10.1029/2018JG004637, 2018.

Peters, A., Nehls, T., Schonsky, H., and Wessolek, G.: Separating precipitation and evapotranspiration from noise – a new filter routine for high-resolution lysimeter data, Hydrology and Earth System Sciences, 18, 1189–1198, https://doi.org/10.5194/hess-18-1189-2014, https://www.hydrol-earth-syst-sci.net/18/1189/2014/, 2014.

Peters, A., Nehls, T., and Wessolek, G.: Technical note: Improving the AWAT filter with interpolation schemes for advanced processing of high resolution data, Hydrology and Earth System Sciences, 20, 2309–2315, https://doi.org/10.5194/hess-20-2309-2016, https://www.hydrol-earth-syst-sci.net/20/2309/2016/, 2016.

Peters, A., Groh, J., Schrader, F., Durner, W., Vereecken, H., and Pütz, T.: Towards an unbiased filter routine to determine precipitation and evapotranspiration from high precision lysimeter measurements, Journal of Hydrology, 549, 731–740, https://doi.org/10.1016/j.jhydrol.2017.04.015, https://linkinghub.elsevier.com/retrieve/pii/S0022169417302330, 2017.

Qubaja, R., Amer, M., Tatarinov, F., Rotenberg, E., Preisler, Y., Sprintsin, M., and Yakir, D.: Partitioning evapotranspiration and its long-term evolution in a dry pine forest using measurement-based estimates of soil evaporation, Agricultural and Forest Meteorology, 281, 107 831, https://doi.org/10.1016/j.agrformet.2019.107831, https://linkinghub.elsevier.com/retrieve/pii/S0168192319304472, 2020.

R Core Team: R: A Language and Environment for Statistical Computing, R Foundation for Statistical Computing, Vienna, Austria, https://www.R-project.org/, 2020.

Reichstein, M., Papale, D., Valentini, R., Aubinet, M., Bernhofer, C., Knohl, A., Laurila, T., Lindroth, A., Moors, E., Pilegaard, K., and Seufert, G.: Determinants of terrestrial ecosystem carbon balance inferred from European eddy covariance flux sites, Geophysical Research Letters, 34, L01 402, https://doi.org/10.1029/2006GL027880, http://doi.wiley.com/10.1029/2006GL027880, 2007.

Ritter, F., Berkelhammer, M., and Beysens, D.: Dew frequency across the US from a network of in situ radiometers, Hydrology and Earth System Sciences, 23, 1179–1197, https://doi.org/10.5194/hess-23-1179-2019, https://www.hydrol-earth-syst-sci.net/23/1179/2019/, 2019.

Rodriguez-Iturbe, I., Porporato, A., Laio, F., and Ridol, L.: Plants in water-controlled ecosystems: active role in hydrologic processes and response to water stress I. Scope and general outline, Advances in Water Resources, p. 11, 2001.

Saaltink, M. W., Kohfahl, C., and Molano-Leno, L.: Analysis of water vapor adsorption in soils by means of a lysimeter and numerical modeling, Vadose Zone Journal, 19, https://doi.org/10.1002/vzj2.20012, https://onlinelibrary.wiley.com/doi/abs/10.1002/vzj2.20012, 2020.

Schneider, J., Groh, J., Pütz, T., Helmig, R., Rothfuss, Y., Vereecken, H., and Vanderborght, J.: Prediction of soil evaporation measured with weighable lysimeters using the FAO Penman–Monteith method in combination with Richards' equation, Vadose Zone Journal, 20, e20 102, 2021.

Schrader, F., Durner, W., Fank, J., Gebler, S., Pütz, T., Hannes, M., and Wollschläger, U.: Estimating Precipitation and Actual Evapotranspiration from Precision Lysimeter Measurements, Procedia Environmental Sciences, 19, 543–552, https://doi.org/10.1016/j.proenv.2013.06.061, https://linkinghub.elsevier.com/retrieve/pii/S1878029613003319, 2013.

Seneviratne, S. I., Corti, T., Davin, E. L., Hirschi, M., Jaeger, E. B., Lehner, I., Orlowsky, B., and Teuling, A. J.: Investigating soil moisture–climate interactions in a changing climate: A review, Earth-Science Reviews, 99, 125–161, https://doi.org/10.1016/j.earscirev.2010.02.004, https://linkinghub.elsevier.com/retrieve/pii/S0012825210000139, 2010.

Sonntag, D.: Important new values of the physical constants of 1986, vapour pressure formulations based on the ITS-90, and psychrometer formulae, Zeitschrift für Meteorologie, 40, 340–344, 1990.

Thom, A. .: Momentum, mass and heat exchange of vegetation, Quarterly Journal of the Royal Meteorological Society, 98, 124–134, 1972.

Tomaszkiewicz, M., Abou Najm, M., Beysens, D., Alameddine, I., and El-Fadel, M.: Dew as a sustainable non-conventional water resource: a critical review, Environmental Reviews, 23, 425–442, https://doi.org/10.1139/er-2015-0035, http://www.nrcresearchpress.com/doi/10.1139/er-2015-0035, 2015.

Tuller, M., Or, D., and Dudley, L. M.: Adsorption and capillary condensation in porous media: Liquid retention and interfacial configurations in angular pores, Water Resources Research, 35, 1949–1964, https://doi.org/10.1029/1999WR900098, http://doi.wiley.com/10.1029/1999WR900098, 1999.

Uclés, O., Villagarcía, L., Moro, M. J., Canton, Y., and Domingo, F.: Role of dewfall in the water balance of a semiarid coastal steppe ecosystem, Hydrological Processes, 28, 2271–2280, https://doi.org/10.1002/hyp.9780, http://doi.wiley.com/10.1002/hyp.9780, 2014.

Uclés, O., Villagarcía, L., Cantón, Y., Lázaro, R., and Domingo, F.: Non-rainfall water inputs are controlled by aspect in a semiarid ecosystem, Journal of Arid Environments, 113, 43–50, https://doi.org/10.1016/j.jaridenv.2014.09.009, https://linkinghub.elsevier.com/retrieve/pii/S0140196314001931, 2015.

Uclés, O., Villagarcía, L., Cantón, Y., and Domingo, F.: Partitioning of non rainfall water input regulated by soil cover type, CATENA, 139, 265–270, https://doi.org/10.1016/j.catena.2015.02.018, https://linkinghub.elsevier.com/retrieve/pii/S0341816215000600, 2016.

Verhoef, A., Diaz-Espejo, A., Knight, J. R., Villagarcía, L., and Fernández, J. E.: Adsorption of Water Vapor by Bare Soil in an Olive Grove in Southern Spain, Journal of Hydrometeorology, 7, 1011–1027, https://doi.org/10.1175/JHM556.1, http://journals.ametsoc.org/doi/10.1175/JHM556.1, 2006.

Weathers, K. C., Ponette-González, A. G., and Dawson, T. E.: Medium, Vector, and Connector: Fog and the Maintenance of Ecosystems, Ecosystems, 23, 217–229, https://doi.org/10.1007/s10021-019-00388-4, http://link.springer.com/10.1007/s10021-019-00388-4, 2020.

Xu, X., Konings, A. G., Longo, M., Feldman, A., Xu, L., Saatchi, S., Wu, D., Wu, J., and Moorcroft, P.: Leaf surface water, not plant water stress, drives diurnal variation in tropical forest canopy water content, New Phytologist, 231, 122–136, https://doi.org/10.1111/nph.17254, https://onlinelibrary.wiley.com/doi/10.1111/nph.17254, 2021.

Yamanaka, T. and Yonetani, T.: Dynamics of the evaporation zone in dry sandy soils, Journal of Hydrology, p. 14, 1999.

Zhang, Q., Wang, S., Yue, P., and Wang, R.: A measurement, quantitative identification and estimation method(QINRW) of non-rainfall water component by lysimeter, MethodsX, 6, 2873–2881, https://doi.org/10.1016/j.mex.2019.11.012, https://linkinghub.elsevier.com/retrieve/pii/S2215016119303152, 2019a.

640 Zhang, Q., Wang, S., Yue, P., and Wang, S.: Variation characteristics of non-rainfall water and its contribution to crop water requirements in China's summer monsoon transition zone, Journal of Hydrology, 578, 124 039, https://doi.org/10.1016/j.jhydrol.2019.124039, https://linkinghub.elsevier.com/retrieve/pii/S0022169419307668, 2019b.

A1 Symbolslist

Symbol	Full form	Unit
C_p	Specific heat capacity of dry air = 1004	$\mathrm{m^2\,m^{-2}\,K^{-1}}$
G	Soil heat flux	$\mathrm{W\,m^{-2}}$
R_{net}	Net radiation	$\mathrm{W\,m^{-2}}$
SWC	Volumetric soil water content	$\mathrm{m^3\,m^{-3}}$
T_a	Air temperature	°C
T_s	Surface temperature	°C
T_{dew}	Atmospheric dewpoint temperature	°C
T_{soil}	Soil temperature	°C
γ	Psychrometric constant	$\mathrm{K^{-1}}$
ρ_a	Density of air	$\mathrm{kg\,m^{-3}}$
s	Slope of the saturation specific humidity curve	$\mathrm{kPa\,K^{-1}}$
ET	Evapotranspiration	mm
G	Ground heat flux	$\mathrm{W\,m^{-2}}$
LW	Long wave radiation	$\mathrm{W\,m^2}$
SW	Short wave radiation	$\mathrm{W\,m^2}$
ΔW	Lysimeter weight change	kg
Ψ	Soil matric potential	hPa
δq	Deficit in specific humidity at reference level	$\mathrm{kg\,kg^{-1}}$
λE	Latent heat flux	$\mathrm{W\,m^{-2}}$
σ	Boltzmann's constant = 5.67×10^{-8}	$\mathrm{W\,K^{-4}\,m^{-2}}$
ε	Emissivity of grass cover = 0.99	NA
e_a	Actual vapor pressure of the atmosphere	hPa
$e_{s,0}$	Vapor pressure of soil air at the soil surface	kPa
rH	Relative humidity	%
r_{av}	Aerodynamic resistance to vapor transport between the surface and air	$\mathrm{s\,m^{-1}}$
u^*	Friction velocity	$\mathrm{m\,s^{-1}}$
u	Wind speed	$\mathrm{m\,s^{-1}}$

A2   Additional equations

645   **Surface temperature (T_s, °C)** was calculated from measurements of the radiometric tower

$$T_s = \sqrt[4]{\frac{LW\downarrow}{\sigma} - \frac{LW\downarrow}{\sigma \times \varepsilon} + \frac{LW\uparrow}{\sigma \times \varepsilon}} - 273.15 \tag{A1}$$

where LW is long wave radiation up ($\uparrow$) and down ($\downarrow$) ($\mathrm{W\,m^{-2}\,s^{-1}}$), σ is Boltzmann's constant ($\mathrm{W\,K^{-4}\,m^{-2}}$) and ε is emissivity of grass (NA).

Dewpoint temperature (T_{dew}, °C) was calculated from rH and T_a based on the Magnus equation ($\lambda = 17.62$, $\beta = 243.12$)
650   (Sonntag, 1990):

$$T_{dew} = \frac{\lambda \times \left(ln\left(\frac{rH}{100}\right) + \frac{\beta \times T_a}{\lambda + T_a} \right)}{\beta - \left(ln\left(\frac{rH}{100}\right) + \frac{\beta \times T_a}{\lambda + T_a} \right)} \tag{A2}$$

where rH is relative humidity (%) and T_a is air temperature (°C).

Evaluation statistics the comparison of the occurrence duration between lysimeter measurements and modeling

Mean absolute error	$mae = \frac{1}{n}\sum\limits_{t=1}^{n} \lvert \hat{y_i} - y_i) \rvert$
Mean squared error	$mse = \frac{1}{n}\sum\limits_{t=1}^{n} (\hat{y_i} - y_i)^2$
Root mean squared error	$rmse = \sqrt{\frac{1}{n}\sum\limits_{t=1}^{n} (\hat{y_i} - y_i)^2}$

Table A2. Evaluation statistics for the comparison of the occurrence duration between lysimeter measurements and modeling. Dew was modeled based on Penman-Monteith (PM) and the equilibrium evaporation model model and adsorption based on the aerodynamic diffusion equation. Statistics are shown for the options i) more than one and ii) more than two lysimeters measuring dew or adsorption, respectively. The units of all values are $\mathrm{hours\,day^{-1}}$.

Flux	Model	#n lysimeters	Length [hour]		
			cor	mae	rmse
Dew	PM	>1	0.44	3.32	4.76
		>2	0.36	3.78	5.30
	Equilibrium evaporation	>1	0.44	3.32	4.76
		>2	0.36	3.78	5.30
Adsorption	Aerodynamic diffusion equation	>1	0.76	4.90	5.8 6
		>2	0.76	4.00	4.70
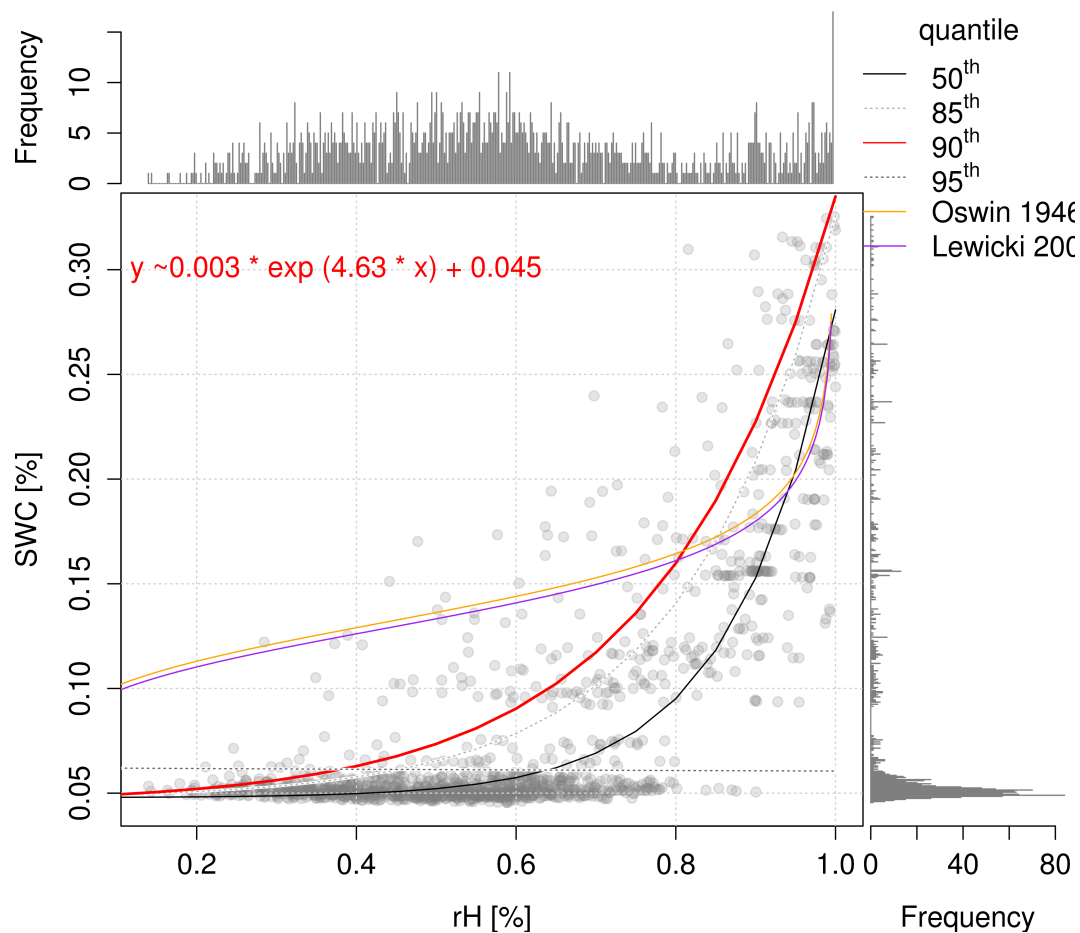
Figure A1. Relationship of SWC and rH during modeled adsorption (gradient driven vapor diffusion towards the soil surface) between April to October. The full formula with the parameters for the 90th quantile from non-linear quantile regression is given in the upper left. The lines additionally illustrate the 50th, 85th, and 95th quantile. Empirical relationships from the literature for equilibrated conditions are shown in orange and purple (Arthur et al., 2016).